An analytical method to approximate the impact of turning on the Macroscopic Fundamental Diagram

By

Guanhao Xu
Department of Civil and Environmental Engineering
The Pennsylvania State University
201 Transportation Research Building
University Park, PA 16802
Phone: 217-974-0536
gux13@psu.edu

Zhengyao Yu
Department of Civil and Environmental Engineering
The Pennsylvania State University
201 Transportation Research Building
University Park, PA 16802
Phone: 814-863-1897
zuy107@psu.edu

Vikash V. Gayah*
Department of Civil and Environmental Engineering
The Pennsylvania State University
231L Sackett Building
University Park, PA 16802
Phone: 814-865-4014
gayah@engr.psu.edu

***Corresponding Author**

April 2020

Word count: 7900

ABSTRACT

Network Macroscopic Fundamental Diagrams (MFDs) have recently been shown to exist in real-world urban traffic networks. The existence of an MFD facilitates the modeling of urban traffic network dynamics at a regional level, which can be used to identify and refine large-scale network-wide control strategies. To be useful, MFD-based modeling frameworks require an estimate of the functional form of a network's MFD. Analytical methods have been proposed to estimate a network's MFD by abstracting the network as a single ring-road or corridor and modeling the flow-density relationship on that simplified element. However, these existing methods cannot account for the impact of turning traffic since only a single corridor is considered. This paper proposes a method to estimate a network's MFD when vehicles are allowed to turn into or out of a corridor. A two-ring abstraction is first used to analyze how turning will impact vehicle travel in a more general network, and then the model is further approximated using a single ring-road or corridor. This approximation is useful as it facilitates the application of existing variational theory-based methods (the stochastic method of cuts) to estimate the flow-density relationship on the corridor, while accounting for the stochastic nature of turning. Results of the approximation compared with a simulation that includes more realistic features that cannot be captured using variational theory—such as internal origins and destinations—suggest that this approximation works at estimating a network's MFD when turning traffic is present.

INTRODUCTION

Relationships between traditional traffic flow metrics averaged across large spatial regions have been explored for decades (*1–3*). These were largely descriptive until a recent study proposed an analytical model that could leverage the existence of well-defined relationships between average network flow (q) and average network density (k)—known more commonly as a network Macroscopic Fundamental Diagram (MFD)—to describe network-wide traffic dynamics (*4*). This analytical model has served as the building block for various frameworks that have been used to develop large-scale network-wide or regional traffic control strategies. A non-exhaustive list of these strategies includes perimeter flow control or gating (*5–11*), congestion pricing (*12–17*), urban road space allocation (*18*, *19*), regional vehicle routing (*20*, *21*) and area-wide signal control plans (*22*, *23*).

These frameworks require knowledge of and are sensitive to the functional form of the MFD. This is not a trivial task as a tremendous amount of data is generally needed for MFD estimation, and there are issues when estimating an MFD empirically using traditional data sources. For example, MFDs derived from loop detector data generally overestimate densities due to standing queues at intersections (*24*). Recent studies have examined how data from GPS-equipped probe vehicles could be fused with traditional detector data to obtain a more accurate estimate of a network's MFD (*25–28*). Due to difficulty in data collection, only a handful of studies have accurately estimated an urban network's MFD using empirical data (*29–32*).

Another approach is to estimate a network's MFD based on its geometric features and traffic control strategies, such as average block length, cycle time, green ratio, free flow speed and link capacity. The original effort in this area applies variational theory (*33*, *34*) to estimate the upper bound of the flow-density relationship of vehicles traveling along a ring-road using the same network parameters (*35*). This method has also been applied within a simulation framework to examine the impact of stochastic topological and signal characteristics (*36*) or bus operations (*37*). Later, extensions to the variational theory method were proposed to tighten the upper bound and better estimate the network's MFD (*38*). Later studies developed additional variational theory-based analytical methods to estimate the MFD of a corridor when the distribution of some network properties (such as link lengths and green times) are known using the stochastic method of cuts (*39*) or for the case in which buses are present (*40*).

Unfortunately, these analytical methods focus on the behavior of vehicles traveling on a single ring-road or corridor and do not capture the impact of vehicles that turn into or out of the corridor at intersections. The existence of turning maneuvers complicates the problem since vehicles now "appear" or "disappear" as they turn into or out of the ring-road or corridor. This violates vehicle conservation along the corridor, and therefore precludes the application of existing kinematic wave theory- or variational theory-based methods for network MFD estimation. A handful of studies have examined the influence of turning maneuvers by abstracting a network by two interconnected ring-roads and used this two-ring system to identify unstable behavior that arises when a network becomes congested (*41–45*). However, these studies fail to provide a method to estimate the functional form of a network's MFD when this turning behavior is included,

which is needed to model network dynamics at a regional level or identify/refine traffic control strategies.

In light of the above, this paper proposes an analytical method to estimate the functional form of a network's MFD when turning vehicles are present. As will be shown here, vehicles that turn into and out of a corridor will change the sequence in which vehicles interact with traffic signals, specifically the signal offsets. Although the turning maneuvers can be modeled using a two-ring system, a single ring-road approximation is proposed that allows the use of existing variational theory-based MFD estimation methods such as the stochastic method of cuts for MFD estimation. Extensions to the stochastic method of cuts are also provided to address the unique impacts of turning traffic.

The remainder of this paper is organized as follows. First, we show how turning vehicles can potentially impact a network's MFD via microscopic simulations. Second, we describe how a network can be abstracted into a system of two ring-roads that incorporates the impact of turning. We then propose a single-ring approximation of a two-ring system that can be used to analytically estimate the MFD when turning is present. The methodology of estimating network MFDs with turning is then discussed in the next section, followed by simulation results validating the analytical model. Finally, some discussion and concluding remarks are provided.

IMPACT OF VEHICLE TURNING ON THE NETWORK MFD

In this section, grid network is simulated using a cellular automata model (CAM) to study the impact of turning vehicles on a network's observed flow-density relationship. The remainder of this section describes the detailed logic of the simulation and the resulting flow-density relationships.

Simulation description

The network simulated here consists of one-way streets arranged into a simple 6 x 6 square grid pattern. Each street has one travel lane on which traffic is assumed to obey a triangular fundamental diagram with a common free flow speed (40 mile/hour), capacity (2000 vehicle/hour) and jam density (250 vehicle/mile). All intersections are assumed to be signalized and share common signal timing properties (e.g., cycle lengths, green times and offsets).

Vehicles on the network were simulated using the cellular automata model (CAM) proposed by Daganzo (*46*), which is consistent with kinematic wave theory (*47–49*). In this framework, each street is broken up into homogeneous discrete cells of length 0.004 miles (equal to average vehicle spacing at jam density) that allow only a single vehicle to occupy any cell at any time period. Vehicle locations are updated at consistent intervals of 0.36 seconds. Average flow and density across the entire network are computed using the generalized definitions proposed by Edie (*50*) at discrete intervals of 6 minutes.

The simulation starts with vehicles uniformly distributed across so that the average density on each link is approximately the same. To maintain a constant density throughout the simulation, periodic boundary conditions are maintained in which vehicles exiting the network at the downstream-most point of a given street are reinserted at the upstream-most point of that street. Vehicles travel through the network and turn randomly with some fixed probability p at each intersection. To simulate internal traffic, vehicles also have a probability of completing their trip and exiting the network at the midpoint of each block. The average probability of completing inside the network is pre-determined in the simulation (all results shown in this paper are for an average value of 10%, but the observations are consistent across different exiting probabilities). However, the probability of a vehicle exiting on a specific link in the network is proportional to that link's density. This was done to represent more realistic network behavior in which busier areas attract more trips than less busy areas. Since a constant density is maintained inside the network, vehicles that complete their trip are inserted elsewhere in the network to represent a new trip origin.

Simulation results

FIGURE 1 provides the observed flow-density relationship for the grid network obtained from the simulations with different turning probabilities at the intersections. FIGURE 1a provides observed flow-density pairs for a network with relatively short blocks, while FIGURE 1b provides observed flow-density pairs for a network with relatively long blocks. Settings for the short block network are individual block lengths of 0.48 mile, cycle lengths of 72 seconds, equal green time of 36 seconds provided to both competing directions, and signal offsets equal to zero. Settings for the long block network are individual block lengths of 0.96 mile, cycle lengths of 90 seconds, equal green time of 45 seconds provided to both competing directions and signal offsets equal to zero.

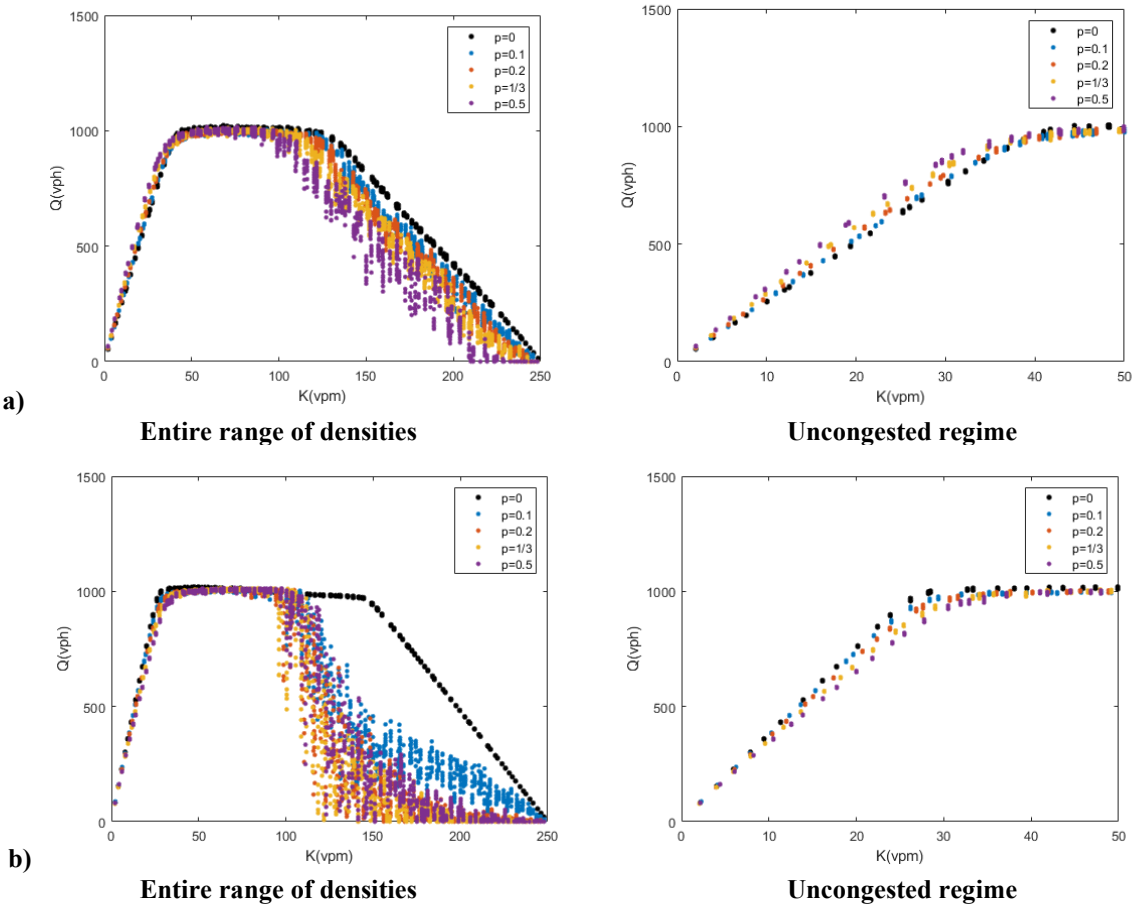

FIGURE 1 (a) MFD of a short-block network for various values of turning ratio, (b)MFD of a long-block network for various values of turning ratio.

In both cases, the observed flow-density relationships are very well-defined in the uncongested and capacity states, but become scattered in congestion. This phenomenon occurs due to the tendency toward inhomogeneous vehicle distributions when the network is congested (*42*, *51*). In this congested regime, it is likely that the MFD is not reflective of the observed flow-density relationship but instead serves as an upper bound for the expected flow-density relationship.

Therefore, we focus here on the more well-defined uncongested and capacity regimes of the observed flow-density relationship, which is more indicative of its MFD. Notice that the presence of turning does not impact the network's capacity: in all cases, the same capacity of 1000 vehicles/hour is maintained. However, observed flows in the free flow branch when turning is present ($p > 0$) differ from those when there is no turning ($p = 0$) and does so in different ways. For the settings used here, observed flows (and thus average speeds) increase with p when blocks are short; however, observed flows (and thus average speeds) decrease with p when blocks are long. Additionally, the lowest density for which the network reaches capacity changes when turning is present and again does so in different ways depending on if blocks are short or long.

Thus, we see that the presence and amount of turning impact the functional form of the MFD. Possible explanations for this behavior are explored in the following section, which uses a two ring-road network abstraction to study this behavior.

ABSTRACTING A GRID NETWORK TO MODEL TURNING TRAFFIC

In this section, we propose a simple two ring-road network model that provides a possible explanation for simulation results observed in the previous section and then use this explanation to obtain a method for analytically approximating a network's MFD when turning is present. For simplicity, this discussion will focus on the behavior of homogeneous networks in which: 1) all links share the same properties—i.e., blocks are of the same length so the grid is square; 2) the fundamental diagram relating traffic flow, and vehicular density is the same on each link; and, 3) signal offsets between adjacent intersections are zero. However, these assumptions are made for illustrative purposes and the logic can be extended to more general situations.

Single and two ring abstractions of a grid network

Existing analytical methods to estimate a network's MFD abstract a traffic network into a single ring-road on which vehicles can travel continuously and estimate an upper-bound for the flow-density relationship on that ring-road. To illustrate this abstracting, consider the left-hand side of FIGURE 2a, which shows a grid network made up of one-way streets with alternating directions. Under the conditions described above, the behavior of this simple grid network can be represented by a ring-road created by bending one of the links as shown on the right-hand side of FIGURE 2a. However, this simple, single-ring abstraction assumes that the traffic profile on each link in the grid network is the same and cannot accommodate vehicles turning into and out of the ring-road. For this reason, it does not accommodate turning maneuvers in the network.

Vehicles turning at intersections of the grid network described above will change from one perpendicular direction (for example and without loss of generality, north-south) to another (e.g., east-west). Thus, in order to capture the impacts of turning traffic, the behavior of vehicles on north-south and east-west streets need to be considered separately. If we assume now that turns are perfectly correlated at each intersection (i.e., when a vehicle turns from a link traveling one perpendicular direction to another at an intersection, this same maneuver occurs at all other intersections simultaneously), then this grid network can be abstracted into a system of two ring-roads that are connected by a traffic signal as in FIGUE 2b. This simple system mimics the behavior of the grid system but allows turning as vehicles are allowed to turn/switch between the rings at the point of tangency that reflects the intersection.

Previous studies have used this simple two-ring network abstraction to unveil key features about urban transportation networks, including the presence of bifurcations in the MFD, network instability and the beneficial impact of adaptive driver routing and adaptive traffic signal control (*41–43*). However, the MFD of this two-ring system (or any corridor with turning traffic) is

difficult to estimate analytically since conservation is violated within each of the rings. Specifically, vehicles turning into or out of a link at the intersection will be "created" or "destroyed" at the intersection and these existing methods cannot explicitly account for this. One related study combined a kinematic wave model with a merge/diverge model to develop an analytical solution, but did not account for the presence of traffic signals (*44*). Another applied a link-queue model to study general features of the system with traffic signals but could not analytically estimate the network's MFD (*45*).

This paper proposes a way to approximate vehicle behavior in this two-ring system using a single ring-road that accurately portrays how vehicles would move through the two-ring network when turning is present. The benefit of this approximation is that existing analytical approaches, such as variational theory and the stochastic method of cuts, can then be applied to this approximately equivalent single ring network to estimate its MFD. The following section describes the details of this single-ring approximation.

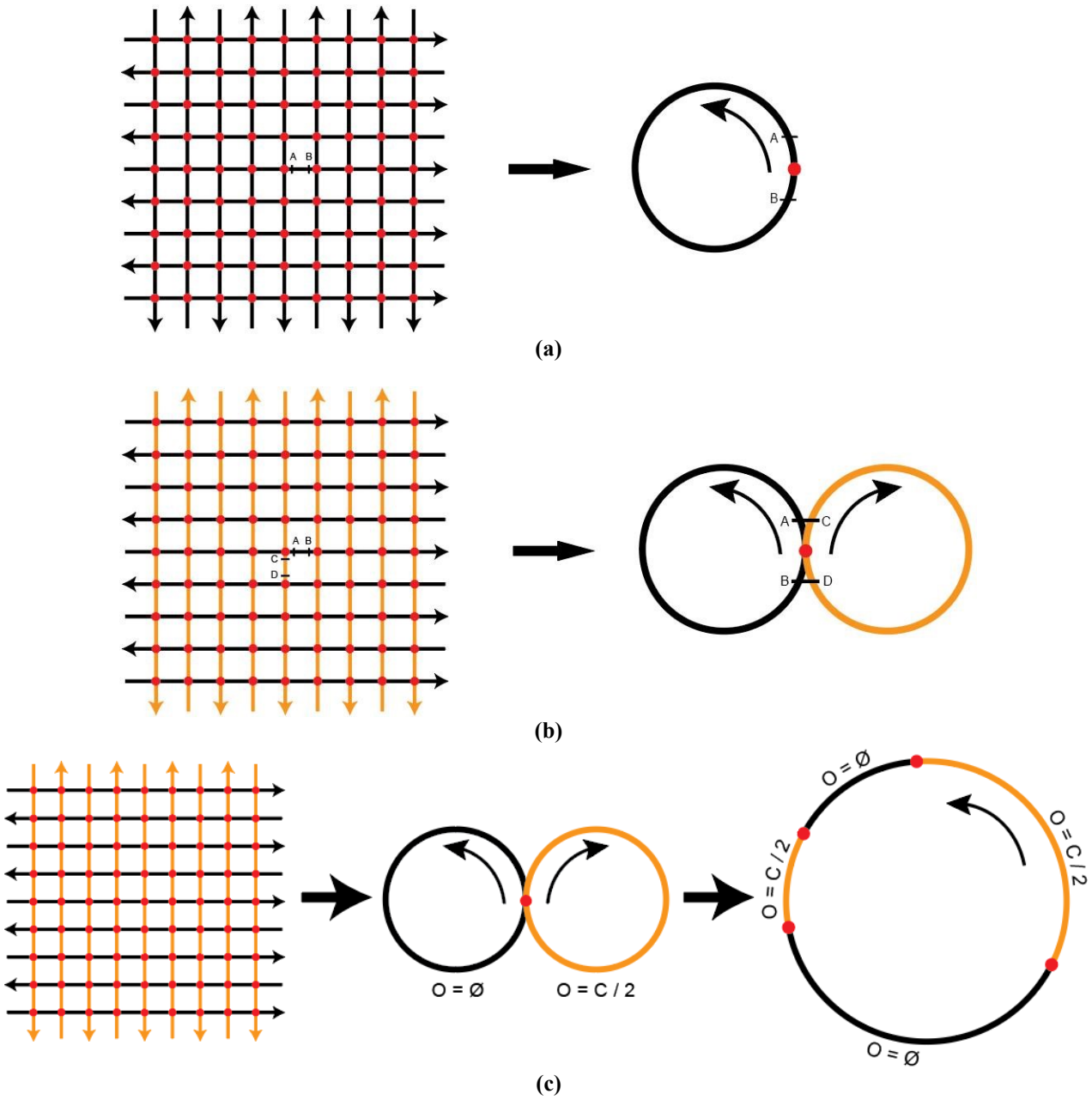

FIGURE 2. (a) Single ring-road abstraction of a grid network; (b) Two ring-road abstraction of a grid network; and, (c) Single-ring approximation of a grid network accounting for turning.

Single-ring approximation of two-ring network

The single ring approximation of the two-ring network works by noting that turning from one ring to another changes how a vehicle interacts with traffic signals. The left-hand side of FIGURE 3a shows a time-space diagram of the traffic signal patterns a vehicle encounters along one of the two rings, which represents travel on one of the two perpendicular directions in the grid network. The red bars show the time periods that the traffic signal is red for the direction of travel. Note that

these red periods also represent the time when the traffic signal is green for the conflicting direction. The dotted line represents the trajectory of the first vehicle discharged after the signal turns green. Notice that this vehicle only travels a single block before it arrives at the following intersection during its red phase and must stop.

When a vehicle makes a turning maneuver and moves from one direction to the other, it will move from a link traveling in one direction to a link traveling in the other. This will then change the sequence in which the vehicle encounters (and interacts with) red signal phases at subsequent intersections. The left-hand side of FIGURE 3b represents the case where this vehicle turns at each intersection. After each turn is made, the red period that the vehicle encounters changes since the red period for one travel direction is equal to the green period for the other. This vehicle that turns at each intersection now travels five blocks before stopping. As a result, average travel speeds (and thus flow) increases because of the turns.

Of course, the reverse may also be true. The right-hand side of FIGURE 3a and FIGURE 3b represent the case in which this vehicle would have experience almost no delays at the intersections if it did not turn (FIGURE 3a), but now becomes periodically stopped by a red phase for a long time due to the turning maneuvers (FIGURE 3b). Under such circumstances, turning would cause travel speeds (and thus flow) to decrease.

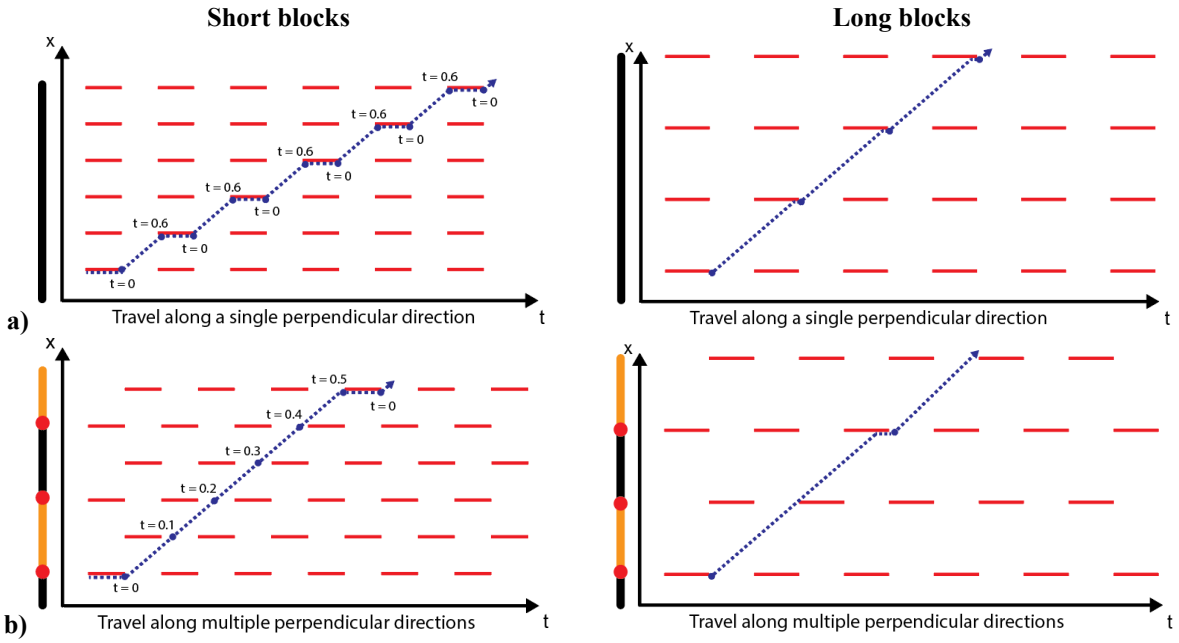

FIGURE 3. (a) Time-space diagram of an observer traveling on a single perpendicular direction on a grid network; (b) time-space diagram of an observer traveling on two perpendicular directions on a grid network.

Thus, it appears that vehicular behavior when turning traffic is present can be approximated as travel along a single corridor by simply adjusting the signal timing patterns. This approximation

is graphically illustrated in FIGURE 2c. The single ring-road can be divided into unique alternative segments, each representing travel on one of the two ring-roads. These individual segments are separated by the intersections where a turning maneuver is performed. Signals on segments representing one set of perpendicular roads have a different offset compared to those on segments representing the other set of perpendicular roads. In general, the offsets in each segment would simply differ by half of the cycle length; for the assumptions made in this section, this represents an offset of zero for travel on one ring and one-half of the cycle length for travel on the other. Thus, the network with turning traffic can be modeled using a single ring-road by appropriately considering the lengths of each of these individual segments, as demonstrated in the next section.

ANALYTICAL APPROXIMATION FOR MFD

In this section, we propose an analytical method to estimate the network MFD when turning is present. Here, we assume that vehicles have a fixed probability p of turning onto the perpendicular street when they pass through each intersection. Thus, any individual vehicle may travel a unique number of intersections before turning. In this scenario, the length of each segment on the single ring approximation (shown in FIGURE 1c) would be stochastic. One recently proposed method to overcome such a challenge is the stochastic method of cuts recently proposed in (*39*) to estimate the MFD of a single corridor traffic network when network features vary randomly. Unfortunately, this study only provides analytical formulas to estimate the MFD when red time, green time and block length are drawn randomly from a known distribution. However, incorporating the impacts of turning traffic requires that signal offsets vary when moving from one segment of the corridor to another and these changes are not random *within* each segment: they only change when a vehicle performs a turning maneuver and would stay changed until another turning maneuver is performed. Thus, in this paper, we expand the stochastic method of cuts to accurately account for this situation.

The stochastic method of cuts (*39*) relies on estimating the travel time (Y) of and number of vehicles passing (X) a set of observers as they travel through a corridor between departures at the start of a green signal period. Three types of observer travel strategies (s) are considered:

- s_0: observer stays at the same intersection
- s_1: observer travels at speed v_f, stops at any red phase, and stays at that intersection until the beginning of the red.
- s_2: observer travels at speed v_f but stops at every intersection.

Note that we only describe the movement of observers traveling in the forward direction since the portion of the MFD obtained using backward-moving observers can be found similarly, as described in (*39*). The flow-density relationship provided by any strategy s, $q_S(k)$, is normal with mean μ_s and variance σ_s^2/t:

$$\mu_s = \frac{\mu_X}{\mu_Y} \quad (1)$$

$$\sigma_s^2 = \frac{Var[X-\mu_s Y]}{\mu_Y} \quad (2)$$

where:

$$Var[X-\mu_s Y] = \sigma_X^2 + \mu_s^2\sigma_Y^2 - 2\mu_s cor(X,Y).\mu_X\mu_Y \quad (3)$$

$$X = L \times k + Q \times G \quad (4)$$

$$Y = \frac{L}{v_f} + G + R \quad (5)$$

and L is the total length traveled in one period between starting at green initiations, k is the density at which the flow will be estimated, Q is the roadway capacity, G is the time an observed is stopped during the green signal indication, and R is the time an observer is stopped during the red signal indication.

This information can be used to obtain the CDF of $q_S(k)$ for each strategy s, $F_{s,k}(q)$. From this, the CDF of the overall flow-density relationship, $F_{q(k)}(q)$, is provided from the CDF of the minimum of these strategies:

$$F_{q(k)}(q) = 1 - \prod \ (1 - F_{s,k}(q)) \quad (6)$$

This CFD can be used to obtain various percentiles of the MFD. The remainder of this section provides details on how to estimate the parameters μ_X, μ_Y, σ_X^2, σ_Y^2 and $cor(X,Y)$ needed to obtain the MFD under each observer strategy. The remainder of this section describes how to compute these terms for each of the three strategies when applying the single-ring approximation for the two-ring system with turning.

Strategy s_0

Under Strategy s_0, an observer will always stay at the same intersection. Since the green time here is deterministically set to one-half of the cycle length at all intersections, the derivation of the parameters is relatively straightforward. For example, L is always 0 and the observer always spends half of the cycle length stopped during the green and red signal indications; i.e., $G = R = C/2$. Thus, we find that:

$$\mu_{X\_s_0} = 0 \times k + Q \times \frac{C}{2} = \frac{QC}{2} \quad (7)$$

$$\sigma_{X\_s_0}^2 = 0 \quad (8)$$

$$\mu_{Y\_s_0} = \frac{0}{v_f} + \frac{C}{2} + \frac{C}{2} = C \quad (9)$$

$$\sigma^2_{Y_{s_0}} = 0 \quad (10)$$

Note that $cor(X,Y)$ is not needed since $\sigma^2_{X\_s_0} = \sigma^2_{Y_{s_0}} = 0$.

Strategy s_1

Under Strategy s_1, the observer never stops during a signal's green indication; thus, $G = 0$. Further, since block lengths are assumed to be constant, the number of vehicles passing an observer can be written as a function of the average block length (l) and the number of blocks an observer travels (n):

$$X = n \times l \times k + Q \times 0 = nlk \quad (11)$$

From this:

$$\mu_{X\_s_1} = \mu_n l\, k \quad (12)$$

$$\sigma^2_{X\_s_1} = \sigma^2_n . (l.k)^2 \quad (13)$$

We now propose a method to determine μ_n and σ^2_n. This method starts by identifying the set of possible times that an observer may depart from an intersection during its green period or arrive to an intersection during its red period, M. This set is finite for cases in which the fraction of a cycle length it takes an observer to travel between two intersections, $L/(v_f.C)$, and the ratio of offset to cycle length, O/C , are rational numbers. We can define each of these unique times $m \in M$ by amount of time deviation from the beginning of the most recent green initiation at that signal, expressed as a fraction of a cycle length. Denote this t_m and note that $t_m \in [0,1)$. The left side of FIGURE 3 provides examples for the case in which $L/(v_f.C) = 0.6$ and O = 0. In Figure 3a, the vehicle/observer leaves the signal at the beginning of the green signal, so $t = 0.0$ at the first intersection. Since it takes the observer 0.6 cycle lengths to travel a block, the t for intersection two is 0.6. However, since the observer stops at this intersection, the process repeats itself and $t = 0.6$ at all subsequent intersections. In Figure 3b, again $t = 0.0$ at the first intersection. However, the observer takes 0.6 cycle lengths to reach the next intersection whereas the red period at this intersection lasts for the 0.5 cycle lengths of this travel. Thus, $t = 0.6 - 0.5 = 0.1$ at the second intersection. At the third intersection, $t = 0.2$ since it takes the observer 0.6 cycle lengths to travel the length of the block whereas the red period at this intersection lasts for the 0.5 cycle lengths of this travel.

We now treat the movement of an observer through the corridor as a discrete Markovian Process in which the states are the set of times, M. If an observer arrives at an intersection during its green indication, we call this a transient state since the observer can keep moving towards the next intersection. These transient states occur if $t_m < 0.5$ at that intersection, where 0.5 is the fraction of the cycle that gets a green indication. If an observer arrives to the signal during its red

indication, we call this an absorbing state because it must stop and wait until it can discharge again at 0, repeating its process of travel. These absorbing states occur if $t_m \geq 0.5$.

We now write a transition matrix to describe how an observer changes between states as it moves along the corridor. If an observer is currently at a transient state m, the observer will move to a state associated with time $t_m + L/(v_f.C) - O/C$ with probability $1-p$ and will move to the state associated with $t_m + L/(v_f.C) - O/C + 0.5$ with probability p. The former represents an observer not turning and thus the offset of the downstream signal not changing, while the latter represents the observer making a turning maneuver and thus experiencing the signal with a modified offset. If state m is an absorbing state, we assume that the observer stays in that state m. An example of this matrix for the case in which $L/(v_f.C) = 0.6$ and $O = 0$ is provided in TABLE 1.

TABLE 1. Example of Markov Chain transition matrix for strategy $\mathbf{s_1}$

		Next t_m value									
		0.0	**0.1**	**0.2**	**0.3**	**0.4**	**0.5**	**0.6**	**0.7**	**0.8**	**0.9**
Current t_m value	**0.0**	0	p	0	0	0	0	$1-p$	0	0	0
	0.1	0	0	p	0	0	0	0	$1-p$	0	0
	0.2	0	0	0	p	0	0	0	0	$1-p$	0
	0.3	0	0	0	0	p	0	0	0	0	$1-p$
	0.4	$1-p$	0	0	0	0	p	0	0	0	0
	0.5	0	0	0	0	0	1	0	0	0	0
	0.6	0	0	0	0	0	0	1	0	0	0
	0.7	0	0	0	0	0	0	0	1	0	0
	0.8	0	0	0	0	0	0	0	0	1	0
	0.9	0	0	0	0	0	0	0	0	0	1

Transition matrices of this form can be re-written using their canonical form as follows:

$$P = \begin{bmatrix} I & O \\ R & Q \end{bmatrix} \tag{14}$$

where I is the identity matrix, O is a submatrix that consists entirely of 0's, R is the submatrix that deals with the transition from a transient state to an absorbing state and Q is a submatrix that deals with only transient states. The element in the i^{th} row and the j^{th} column of Q^k ($k = 0,1,2 \ldots$) provides the probability of moving between state i to state j after k step (i.e., traveling k blocks). It can also be considered as the expected number of times an observer ends up at state j after traveling k blocks when starting from state i. The elements of $\sum_{k=0}^{\infty} Q^k$ provides the expected number of times an observer visits state j before being absorbed if starting from state i. From (*52*), we find that:

$$\tau = E(\{n_i\}) = (I - Q)^{-1}.\zeta \tag{15}$$

where τ is column vector showing the mean number of steps before being absorbed if starting from each state, ζ is a column vectors composed of all 1's and n_i is the number of states visiting (i.e., blocks traveled) before entering and absorbing state when starting from state i and is used to obtain μ_n. Finally, from σ_n^2 is determined using the following (*52*):

$$var(\{n_i\}) = (2((I-Q)^{-1}) - I)\tau - \tau_{sq} \quad (16)$$

where τ_{sq} is a vector obtained from squaring all the element in τ.

To determine $\mu_{Y\_s_1}$ and $\sigma^2_{Y\_s_1}$, we first split up an observer's travel time into two parts: the time spent moving, Y_m, and the time spent stopped, Y_s,. The time spent moving can be easily calculated as:

$$Y_m = \frac{n.l}{v_f} \quad (17)$$

where n is the number of blocks traveled, l is the length of one block, v is the speed of the observer (either v_f or w). Since we already have derived μ_n and σ_n^2 in section 3.2.1, we can use the previous results to obtain:

$$\mu_{Y_m} = \frac{\mu_n.l}{v_f} \quad (18)$$

$$\sigma^2_{Y_m} = \frac{\sigma_n^2.l^2}{v_f^2} \quad (19)$$

The time spent stopping is simply the remaining part of a cycle when an observer stops at the red. For any absorbing state m, the time spent stopped, Y_{s_m}, is equal to the $1 - t_m$. Let p_m represent the probability that an observer ends up in absorbing state m. Then:

$$\mu_{Y_S} = \sum_m p_m(Y_{s_m}) \quad (20)$$

$$\sigma^2_{Y_s} = \sum_m p_m\left(Y_{s_m} - \mu_{Y_S}\right)^2 \quad (21)$$

Finally:

$$\mu_{Y\_s_1} = \mu_{Y_m} + \mu_{Y_S} \quad (22)$$

$$\sigma^2_{Y\_s_1} = \sigma^2_{Y_m} + \sigma^2_{Y_s} + 2cor(Y_m, Y_s)\sigma_{Y_m}\sigma_{Y_s} \quad (23)$$

In general, the time spent moving and the time spent stopping should not necessarily be correlated. Therefore, we assume that $cor(Y_m, Y_s) = 0$ for simplicity of calculation. This assumption was tested using numerous simulations and found to be appropriate in most cases. Thus,

$$\sigma_{Y\_s_1}^2 = \sigma_{Y_m}^2 + \sigma_{Y_s}^2 \quad (24)$$

Finally, $cor(X, Y)$ is assumed to be 1 as numerical simulation experiments indicate that this quantity is between 0.99 and 1 for all cases tested.

Strategy s_2

Under Strategy 2, an observer will travel at speed v_f between intersections but stop at every intersection and stay there until the beginning of the red. Thus, the distance travelled between each starts L should be fixed to the block length l and X is determined only by the remaining portion of the green, G:

$$X_{s_2} = l.k + Q.G \quad (25)$$

Since G is the only variable and is linear with respect to X, the mean of X can be calculated as:

$$\mu_{X\_s_2} = l.k + Q.\mu_G \quad (26)$$

Since the offset experienced at the next intersection is 0 with probability $1 - p$ (no turn) and 0.5 with probability p (turn), G follows a Bernoulli distribution. We now consider the following two cases with two conditions:

- If $mod(L/(v_f.C) - O/C, 1) < 0.5$, then an observer that does not turn (probability $1 - p$) will experience $G = (0.5 - mod(L/(v_f.C) - O/C, 1)) \times C$ whereas an observer than does turn (probability p) will experience $G = 0$.
- If $mod(L/(v_f.C) - O/C, 1) \geq 0.5$, then an observer that does not turn (probability $1 - p$) will experience $G = 0$ whereas an observer than does turn (probability p) will experience $G = (1 - mod(L/(v_f.C) - O/C, 1)) \times C$.

Therefore X can be derived from a Bernoulli distribution as follows:

$$\mu_G = \begin{cases} (1-p) \times \left((0.5 - mod(L/(v_f.C) - O/C, 1)) \times C\right) + p \times 0 & \text{mod } (L/(v_f C) - O/C, 1) < 0.5 \\ (1-p) \times 0 + p \times ((1 - mod(L/(v_f.C) - O/C, 1)) \times C) & \text{mod } (L/(v_f C) - O/C, 1) \geq 0.5 \end{cases} \quad (27)$$

$$\sigma_G^2 = \begin{cases} (1-p) \times \left((0.5 - mod(L/(v_f.C) - O/C, 1)) \times C - \mu_G\right)^2 \\ +p \times (0 - \mu_G)^2 \end{cases} \quad \text{mod } (L/(v_f C) - O/C, 1) < 0.5$$
$$\begin{cases} p \times \left((1 - mod(L/(v_f.C) - O/C, 1)) \times C - \mu_G\right)^2 \\ +(1-p) \times (0 - \mu_G)^2 \end{cases} \quad \text{mod } (L/(v_f C) - O/C, 1) \geq 0.5 \tag{28}$$

Since G is linear with respect to X, we have:

$$\mu_{X\_s_2} = l.k + Q.\mu_G \tag{29}$$

$$\sigma^2_{X\_s_2} = Q^2.\sigma_G^2 \tag{30}$$

Likewise, Y also follows a Bernoulli distribution with parameter equals to the turning ratio p. The derivation has been omitted for simplicity but follows the same logic as above. The result is:

$$\mu_Y = \begin{cases} (1-p) \times (C \times ceil\left(L/(v_f.C) - O/C\right) + O) \\ +p \times \left(C \times (ceil\left(L/(v_f.C) - O/C\right) + O - 0.5)\right) \end{cases} \quad \text{mod } (L/(v_f C) - O/C, 1) < 0.5$$
$$\begin{cases} (1-p) \times (C \times ceil\left(L/(v_f.C) - O/C\right) + O) \\ +p \times \left(C \times (ceil\left(L/(v_f.C) - O/C\right) + O + 0.5)\right) \end{cases} \quad \text{mod } (L/(v_f C) - O/C, 1) \geq 0.5 \tag{31}$$

$$\sigma_Y^2 = \begin{cases} (1-p)\left(C \times ceil\left(L/(v_f.C) - O/C\right) + O - \mu_Y\right)^2 \\ +p\left(C \times (ceil\left(L/(v_f.C) - O/C\right) + O - 0.5 - \mu_Y\right)^2 \end{cases} \quad \text{mod } (L/(v_f C) - O/C, 1) < 0.5$$
$$\begin{cases} (1-p)\left(C \times ceil\left(L/(v_f.C) - O/C\right) + O - \mu_Y\right)^2 \\ +p\left(C \times (ceil\left(L/(v_f.C)\right) - 0.5) + O + 0.5 - \mu_Y\right)^2 \end{cases} \quad \text{mod } (L/(v_f C) - O/C, 1) \geq 0.5 \tag{32}$$

Finally, $Var\left[X\_s_2 - \mu_{s_2} Y\_s_2\right]$ can be directly computed in a similar way so that the $cor(X, Y)$ does not have to be calculated.

VALIDATION OF ANALYTICAL MODEL

In this section, the MFD derived from the analytical method proposed in the previous section is compared with the observed flow-density relationship from the CAM simulation of a grid network described above. FIGURE 4 illustrates the analytically obtained MFDs and the simulated flow-density relationships for the short block case (FIGURE 4a) and long block case (FIGURE 4b) for various turning probabilities. In each figure, the 10th, 50th and 90th percentile values of the analytically derived MFD are compared to the observed flow-density relationship obtained from the CAM simulation. The results show a remarkable consistency between the analytically obtained

and simulated flow-density relationship in the uncongested and capacity regimes in which the network behavior is stable. In all cases shown and tested, the observed flow-density pairs fall between the 10^{th} and 90^{th} percent confidence interval values. The relative errors between the 50^{th} percentile flows obtained from the analytical approximation and the average simulated flow as a function of density for the MFDs provided in FIGURE 4 were also computed for the uncongested and capacity regimes. These errors were very small and generally fall within 5%, which indicates good consistency between the analytical model and simulation results. This is true even for cases in which offsets are non-zero. The analytical model also predicts the overall trend of increasing flow in the uncongested regime with turning probability for the short block case and decreasing flow in the uncongested regime with turning probability for the long block case.

When it comes to the congested branch, the analytical results no longer match the observed relationships so closely. The observed flow-density relationship generally falls below the upper bound provided by the derived MFD due to inhomogeneous congestion distributions. It appears that the results of these inhomogeneous distributions—which are generally expected in large grid networks like the one simulated here (*42*)—are stronger than the impacts due to how turning vehicles interact with signals in congested networks. While the MFD provides an upper-bound for the flow-density relationship of the network, the actual network performance is usually below the MFD in congested states due to its inhomogeneity. However, as described in (*39*), observed flow-density pairs on the congested branch can be obtained from those in uncongested branch by leveraging symmetry. Since the analytical estimate for the network's MFD match the simulation results in the uncongested branch, it follows that the same would be true when the network operates in congestion provided that behavior is stable.

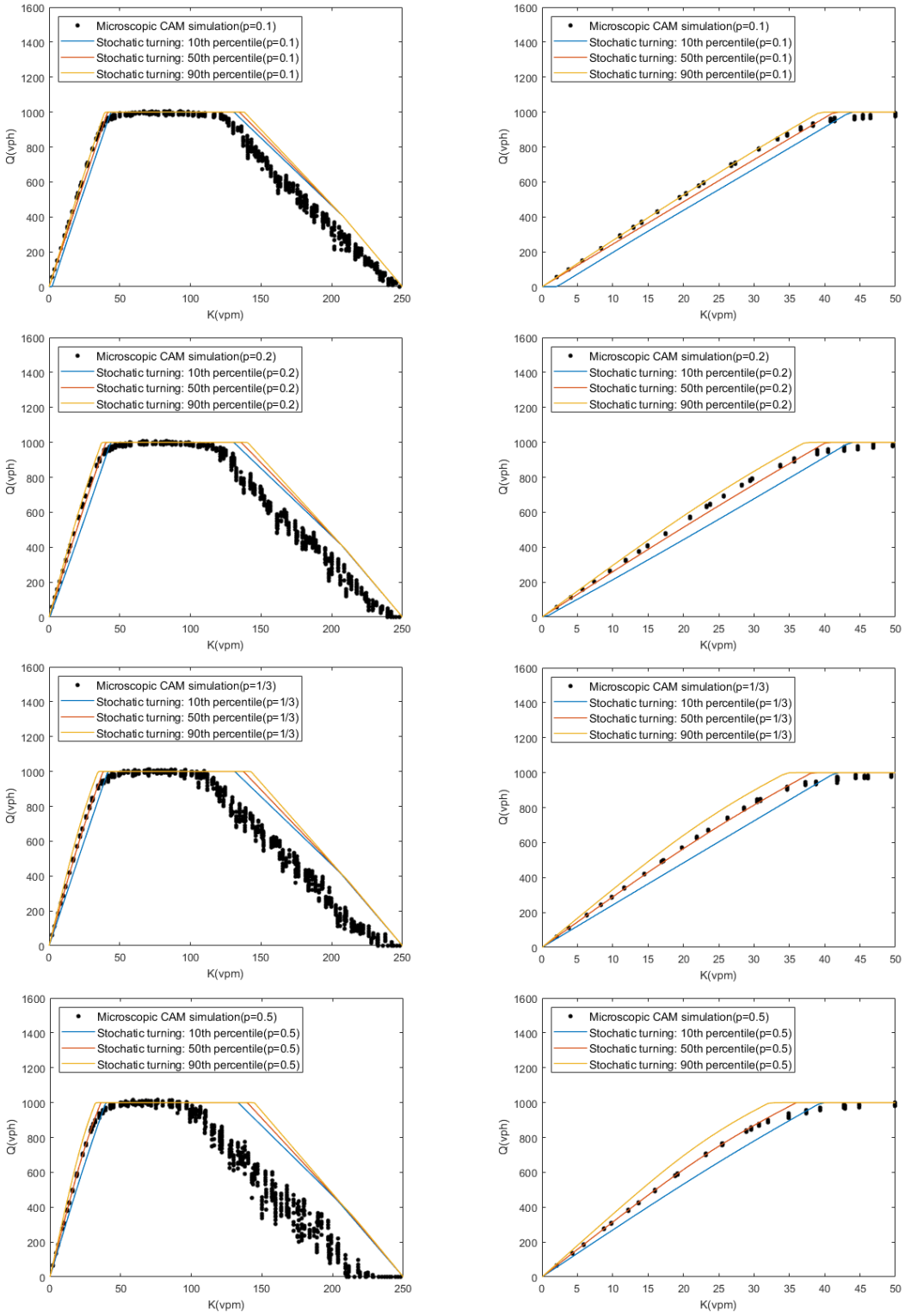
Microscopic CAM simulation(p=0.1)
Stochatic turning: 10th percentile(p=0.1)
Stochatic turning: 50th percentile(p=0.1)
Stochatic turning: 90th percentile(p=0.1)
Microscopic CAM simulation(p=0.2)
Stochatic turning: 10th percentile(p=0.2)
Stochatic turning: 50th percentile(p=0.2)
Stochatic turning: 90th percentile(p=0.2)
Microscopic CAM simulation(p=1/3)
Stochatic turning: 10th percentile(p=1/3)
Stochatic turning: 50th percentile(p=1/3)
Stochatic turning: 90th percentile(p=1/3)
Microscopic CAM simulation(p=0.5)
Stochatic turning: 10th percentile(p=0.5)
Stochatic turning: 50th percentile(p=0.5)
Stochatic turning: 90th percentile(p=0.5)
Q(vph)
K(vpm)

(a)

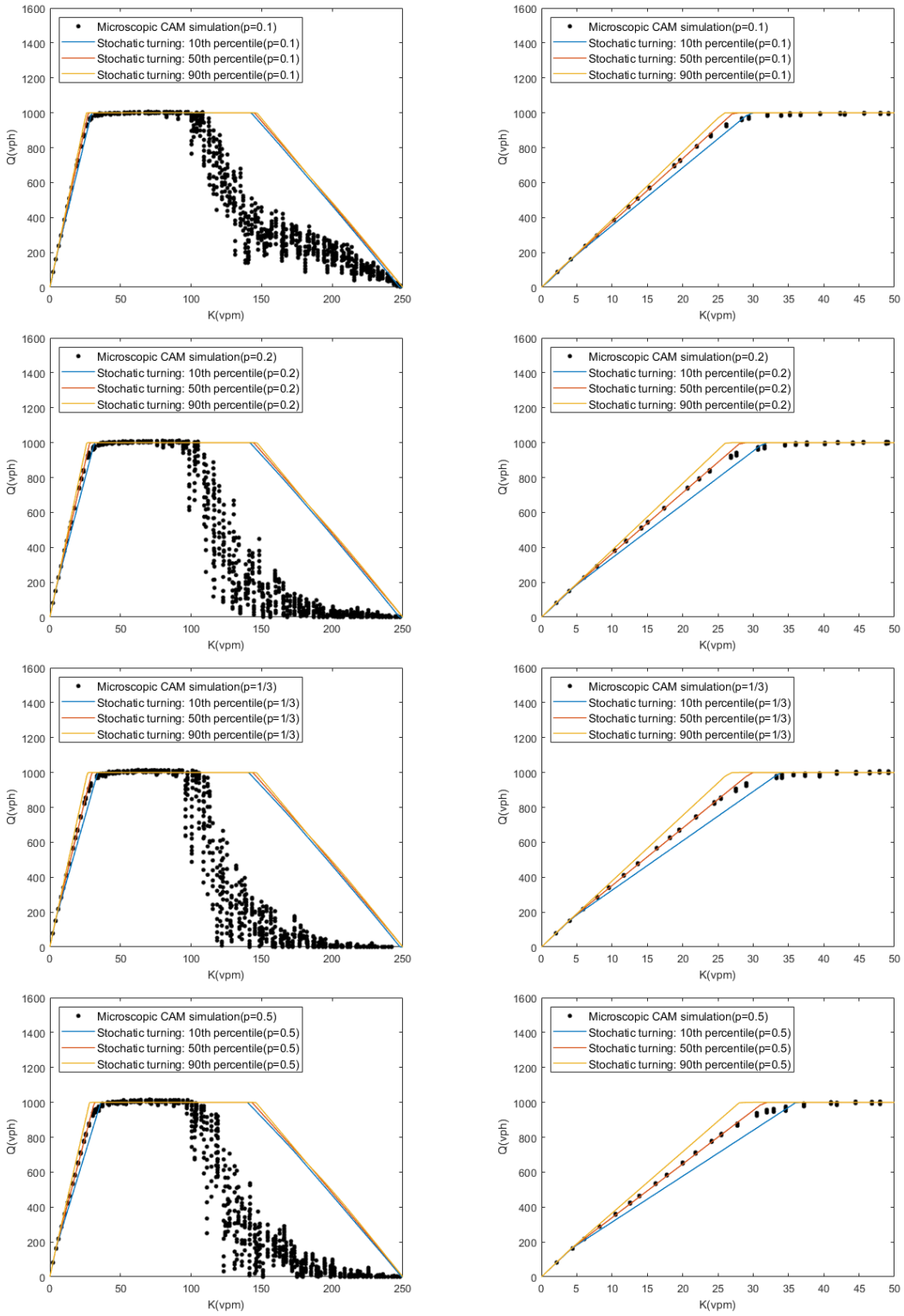

(b)

FIGURE 4. Comparison of analytical MFDs and observed flow-density relationship for different values of *p* in (a) short-block scenario; and, (b) long block scenario.

DISCUSSION AND CONCLUDING REMARKS

This paper provides an analytical method to estimate the impact of turning maneuvers on the functional form of a network's Macroscopic Fundamental Diagram. This analytical method relies on abstracting the network as a single ring-road or corridor and applying the stochastic method of cuts to estimate its MFD. The single ring-road differs from previous works as it explicitly considers how vehicles would interact with traffic signals while traveling in a network and turning between two sets of perpendicular streets. New extensions to the stochastic method of cuts were proposed to accommodate this situation by modeling a vehicle's movement through the network as a Markovian process. MFD estimates obtained from the proposed analytical methods are compared with the observed flow-density relationship obtained from a microscopic simulation of a grid network under more realistic conditions. The impact of trip entrances and exits cannot be captured using existing analytical variational theory methods since they violate vehicle conservation, which serves as a significant limitation to variational theory-based methods.

The simulation results unveil that the presence of turning, even in small amounts, can impact the functional form of the observed flow-density of a network. Specifically, both average speeds (and observed flows for a given density) in the uncongested regime and the density associated with capacity may change when turning maneuvers are present, and both can do so in different ways depending on the network structure. The simulation results also confirm that the proposed method can provide accurate estimates of a networks' observed flow-density relationships when turning is present for the uncongested and capacity regimes. In these two regions, vehicle distributions remain fairly homogeneous in the network and thus the observed relationship is close to the upper bound relationship provided by the MFD. However, the analytical approximation differs from the observed relationship when the network is congested due to the network's tendency towards inhomogeneous congestion distributions and non-MFD producing states. Nevertheless, the proposed analytical method still provides an upper bound on this observed flow-density relationship as would be expected from a network's MFD.

The proposed methods require an estimate of the turning ratio at each intersection, in addition to a general knowledge of network properties (e.g., block lengths, signal timings and fundamental diagram on each link). The former can be reasonably estimated using floating car data by either tracking trajectories in a network to determine how many times a turn is made along a trip or examining trajectories (either using floating car data or with local observations) at individual locations. Such data are becoming more readily available to the research community (*53*). Note also that although it was assumed here that the latter properties were constant, the existing stochastic method of cuts can readily accommodate changes in these properties. Thus, combining the existing methods to apply the stochastic method of cuts with the extension to accommodate random offsets experienced by turning vehicles can provide MFDs for more general networks.

Overall, this paper contributes to the growing research literature on relationships between traffic variables aggregated spatially across traffic networks and how these relationships are influenced by network features. Future work should continue to develop analytical methods to understand how network features will influence these relationships. For example, additional work

should be performed to extend the methods proposed here to accommodate cases in which turning occurs during dedicated signal periods, as opposed to occurring with through movements as assumed here. The movement of conflicting turns, which are often only allowed to move either before or after through vehicles or have to yield to opposing through vehicles, also needs to be examined. Additional work is also needed to understand how these relationships might change when dedicated turning lanes are present.

ACKNOWLEDGEMENTS

This research was supported by NSF Grant CMMI-1749200

AUTHOR CONTRIBUTION STATEMENT

The authors confirm contribution to the paper as follows: study conception and design: G. Xu, Z. Yu, V. V. Gayah; analysis and interpretation of results: G. Xu, Z. Yu, V. V. Gayah; draft manuscript preparation: G. Xu, Z. Yu, V. V. Gayah. All authors reviewed the results and approved the final version of the manuscript.

REFERENCES

1. Godfrey, J. W. The mechanism of a road network. *Traffic Engineering & Control*, Vol. 11, No. 7, 1969, pp. 323–327.

2. Smeed, R. J. The road capacity of city centers. *Traffic Engineering & Control*, Vol. 9, No. 7, 1967, pp. 455–458.

3. Mahmassani, H., J. C. Williams, and R. Herman. Performance of urban traffic networks. Presented at *10th International Symposium on Transportation and Traffic Theory*, 1987.

4. Daganzo, C. F. Urban gridlock: Macroscopic modeling and mitigation approaches. *Transportation Research Part B: Methodological*, Vol. 41, No. 1, 2007, pp. 49–62.

5. Aboudolas, K., and N. Geroliminis. Perimeter and boundary flow control in multi-reservoir heterogeneous networks. *Transportation Research Part B: Methodological*, Vol. 55, 2013, pp. 265–281.

6. Haddad, J., M. Ramezani, and N. Geroliminis. Cooperative traffic control of a mixed network with two urban regions and a freeway. *Transportation Research Part B: Methodological*, Vol. 54, 2013, pp. 17–36.

7. Keyvan-Ekbatani, M., M. Papageorgiou, and I. Papamichail. Urban congestion gating control based on reduced operational network fundamental diagrams. *Transportation Research Part C: Emerging Technologies*, Vol. 33, 2013, pp. 74–87.

8. Keyvan-Ekbatani, M., A. Kouvelas, I. Papamichail, et al. Exploiting the fundamental diagram of urban networks for feedback-based gating. *Transportation Research Part B:*

Methodological, Vol. 46, No. 10, 2012, pp. 1393–1403.

9. Sirmatel, I. I., and N. Geroliminis. Economic Model Predictive Control of Large-Scale Urban Road Networks via Perimeter Control and Regional Route Guidance. *IEEE Transactions on Intelligent Transportation Systems*, Vol. 19, No. 4, Apr. 2018, pp. 1112–1121.

10. Haddad, J., and Z. Zheng. Adaptive perimeter control for multi-region accumulation-based models with state delays. *Transportation Research Part B: Methodological*, Jul. 2018.

11. Yan, F., F. Tian, and Z. Shi. Effects of iterative learning based signal control strategies on macroscopic fundamental diagrams of urban road networks. *International Journal of Modern Physics C*, Vol. 27, No. 4, Apr. 2016.

12. Geroliminis, N., and D. M. Levinson. Cordon pricing consistent with the physics of overcrowding. In *18th International Symposium on Transportation and Traffic Theory*, Springer.

13. Gonzales, E. J., and C. F. Daganzo. Morning commute with competing modes and distributed demand: User equilibrium, system optimum, and pricing. *Transportation Research Part B: Methodological*, Vol. 46, No. 10, 2012, pp. 1519–1534.

14. Gonzales, E. J., and C. F. Daganzo. The evening commute with cars and transit: Duality results and user equilibrium for the combined morning and evening peaks. *Transportation Research Part B: Methodological*, Vol. 57, 2013, pp. 286–299.

15. Simoni, M. D., A. J. Pel, R. A. Waraich, et al. Marginal cost congestion pricing based on the network fundamental diagram. *Transportation Research Part C: Emerging Technologies*, Vol. 56, 2015, pp. 221–238.

16. Yang, K., M. Menendez, and N. Zheng. Heterogeneity aware urban traffic control in a connected vehicle environment: A joint framework for congestion pricing and perimeter control. *Transportation Research Part C: Emerging Technologies*, Vol. 105, Aug. 2019, pp. 439–455.

17. Dantsuji, T., D. Fukuda, and N. Zheng. Simulation-based joint optimization framework for congestion mitigation in multimodal urban network: a macroscopic approach. *Transportation*, Dec. 2019, pp. 1–25.

18. Daganzo, C. F., V. V. Gayah, and E. J. Gonzales. The potential of parsimonious models for understanding large scale transportation systems and answering big picture questions. *EURO Journal on Transportation and Logistics*, Vol. 1, No. 1–2, 2012, pp. 47–65.

19. Zheng, N., and N. Geroliminis. On the distribution of urban road space for multimodal congested networks. *Transportation Research Part B: Methodological*, Vol. 57, 2013, pp. 326–341.

20. Knoop, V. L., S. P. Hoogendoorn, and J. W. C. Van Lint. Routing strategies based on macroscopic fundamental diagram. *Transportation Research Record: Journal of the Transportation Research Board*, Vol. 2315, No. 1, 2012, pp. 1–10.

21. Yildirimoglu, M., and N. Geroliminis. Approximating Dynamic Equilibrium Conditions with Macroscopic Fundamental Diagrams. Presented at *93rd Annual Meeting of the Transportation Research Board*, 2014.

22. DePrator, A., O. Hitchcock, and V. V. Gayah. Improving urban street network efficiency by prohibiting left turns at signalized intersections. *Transportation Research Record: Journal of the Transportation Research Board*, No. in press, 2017.

23. Alonso, B., Á. Ibeas, G. Musolino, et al. Effects of traffic control regulation on Network Macroscopic Fundamental Diagram: A statistical analysis of real data. *Transportation Research Part A: Policy and Practice*, Vol. 126, Aug. 2019, pp. 136–151.

24. Courbon, T., and L. Leclercq. Cross-comparison of macroscopic fundamental diagram estimation methods. *Procedia-Social and Behavioral Sciences*, Vol. 20, 2011, pp. 417–426.

25. Nagle, A. S., and V. V. Gayah. Accuracy of Networkwide Traffic States Estimated from Mobile Probe Data. *Transportation Research Record: Journal of the Transportation Research Board*, No. 2421, 2014, pp. 1–11.

26. Leclercq, L., N. Chiabaut, and B. Trinquier. Macroscopic Fundamental Diagrams: A cross-comparison of estimation methods. *Transportation Research Part B: Methodological*, Vol. 62, 2014, pp. 1–12.

27. Du, J., H. Rakha, and V. V. Gayah. Deriving macroscopic fundamental diagrams from probe data: Issues and proposed solutions. *Transportation Research Part C: Emerging Technologies*, Vol. 66, 2016, pp. 136–149.

28. Ambühl, L., and M. Menendez. Data fusion algorithm for macroscopic fundamental diagram estimation. *Transportation Research Part C: Emerging Technologies*, Vol. 71, Oct. 2016, pp. 184–197.

29. Geroliminis, N., and C. F. Daganzo. Existence of urban-scale macroscopic fundamental diagrams: Some experimental findings. *Transportation Research Part B: Methodological*, Vol. 42, No. 9, 2008, pp. 759–770.

30. Buisson, C., and C. Ladier. Exploring the impact of homogeneity of traffic measurements on the existence of macroscopic fundamental diagrams. *Transportation Research Record: Journal of the Transportation Research Board*, No. 2124, 2009, pp. 127–136.

31. Tsubota, T., A. Bhaskar, and E. Chung. Brisbane macroscopic fundamental diagram: Empirical findings on network partitioning and incident detection. *Transportation Research Record: Journal of the Transportation Research Board*, No. 2421, 2014, pp. 12–21.

32. Knoop, V. L., P. B. C. Van Erp, L. Leclercq, et al. Empirical MFDs using Google Traffic Data. *IEEE Conference on Intelligent Transportation Systems, Proceedings, ITSC*, No. 2018-November, 2018, pp. 3832–3839.

33. Daganzo, C. F. A variational formulation of kinematic waves: Basic theory and complex boundary conditions. *Transportation Research Part B: Methodological*, Vol. 39, No. 2, 2005, pp. 187–196.

34. Daganzo, C. F. A variational formulation of kinematic waves: Solution methods. *Transportation Research Part B: Methodological*, Vol. 39, No. 10, 2005, pp. 934–950.

35. Daganzo, C. F., and N. Geroliminis. An analytical approximation for the macroscopic fundamental diagram of urban traffic. *Transportation Research Part B: Methodological*, Vol. 42, No. 9, 2008, pp. 771–781.

1 36. Geroliminis, N., and B. Boyacı. The effect of variability of urban systems characteristics
2 in the network capacity. *Transportation Research Part B: Methodological*, Vol. 46, No. 10,
3 2012, pp. 1607–1623.

4 37. Boyaci, B., and N. Geroliminis. Estimation of the network capacity for multimodal urban
5 systems. *Procedia - Social and Behavioral Sciences*, No. 16, 2011, pp. 803–813.

6 38. Leclercq, L., and N. Geroliminis. Estimating MFDs in simple networks with route choice.
7 *Transportation Research Part B: Methodological*, Vol. 57, 2013, pp. 468–484.

8 39. Laval, J. A., and F. Castrillón. Stochastic approximations for the macroscopic fundamental
9 diagram of urban networks. *Transportation Research Part B*, Vol. 81, 2015, pp. 904–916.

10 40. Dakic, I., L. Ambühl, O. Schümperlin, et al. On the modeling of passenger mobility for
11 stochastic bi-modal urban corridors. *Transportation Research Part C: Emerging*
12 *Technologies*, Jun. 2019.

13 41. Gayah, V. V., and C. F. Daganzo. Effects of Turning Maneuvers and Route Choice on a
14 Simple Network. *Transportation Research Record: Journal of the Transportation Research*
15 *Board*, No. 2249, 2011, pp. 15–19.

16 42. Daganzo, C. F., V. V. Gayah, and E. J. Gonzales. Macroscopic relations of urban traffic
17 variables: Bifurcations, multivaluedness and instability. *Transportation Research Part B:*
18 *Methodological*, Vol. 45, No. 1, 2011, pp. 278–288.

19 43. Gayah, V. V., X. (Shirley) Gao, and A. S. Nagle. On the impacts of locally adaptive signal
20 control on urban network stability and the Macroscopic Fundamental Diagram.
21 *Transportation Research Part B: Methodological*, Vol. 70, 2014, pp. 255–268.

22 44. Jin, W.-L. W.-L. L., Q.-J. J. Gan, and V. V. Gayah. A kinematic wave approach to traffic
23 statics and dynamics in a double-ring network. *Transportation Research Part B:*
24 *Methodological*, Vol. 57, 2013, pp. 114–131.

25 45. Gan, Q.-J., W.-L. Jin, and V. V. Gayah. Analysis of traffic statics and dynamics in
26 signalized networks: A poincaré map approach. *Transportation Science*, Vol. 51, No. 3,
27 2017.

28 46. Daganzo, C. F. In traffic flow, cellular automata = kinematic waves. *Transportation*
29 *Research Part B: Methodological*, Vol. 40, No. 5, 2006, pp. 396–403.

30 47. Lighthill, M. J., and G. B. Whitham. On kinematic waves. II. A theory of traffic flow on
31 long crowded roads. *Proceedings of the Royal Society of London. Series A. Mathematical*
32 *and Physical Sciences*, Vol. 229, No. 1178, 1955, pp. 317–345.

33 48. Richards, P. I. Shock waves on the highway. *Operations Research*, Vol. 4, No. 1, 1956, pp.
34 42–51.

35 49. Lighthill, M. J., and G. B. Whitham. On kinematic waves. I. Flood movement in long rivers.
36 *Proceedings of the Royal Society of London. Series A. Mathematical and Physical Sciences*,
37 Vol. 229, No. 1178, 1955, pp. 281–316.

38 50. Edie, L. C. Discussion of traffic stream measurements and definitions. Presented at *2nd*
39 *International Symposium on the Theory of Traffic Flow*, 1965.

40 51. Mazloumian, A., N. Geroliminis, and D. Helbing. The spatial variability of vehicle

densities as determinant of urban network capacity. *Philosophical Transactions of the Royal Society A: Mathematical, Physical and Engineering Sciences*, Vol. 368, No. 1928, 2010, pp. 4627–4647.

52. Kemeny, J. G., and J. L. Snell. *Finite Markov Chains*. Spring-Verlag, New York, 1976.

53. Barmpounakis, E., and N. Geroliminis. On the new era of urban traffic monitoring with massive drone data: The pNEUMA large-scale field experiment. *Transportation Research Part C: Emerging Technologies*, Vol. 111, Feb. 2020, pp. 50–71.